

## Modified inderbitzen equipment for simulation of water erosion in undeformed soil samples

Equipamento inderbitzen modificado para simulação da erosão hídrica em amostras de solo indeformado

Andréa Cristina Thoma<sup>1</sup> , Diego Tassinari<sup>1</sup> , Bernat Vinolas Prat<sup>1</sup> , Lauana Lopes dos Santos<sup>1</sup> ,  
Bárbara Pereira Christofaro Silva<sup>2</sup> , Alexandre Christofaro Silva<sup>1</sup> 

### ABSTRACT

Several devices have been developed to assess soil losses by water erosion. However, they rarely assess the combined effects of raindrop impact and surface runoff together with vegetation cover on varying slopes. This study aimed to design and validate an equipment, on laboratory scale, to evaluate the effect of water erosion on undisturbed soil samples with and without plant cover, as well as to assess the kinetic energy of simulated rain and the resultant shear stress at varying runoff intensities. The equipment is composed of a rainfall simulator, an adjustable stand for different slopes and falling heights, and a runoff ramp for testing undisturbed soil samples measuring 15 x 20 x 40 cm (height, width, and length). In this study, the equipment simulated and evaluated the effect of precipitation and runoff on soil losses, allowing to obtain different values of the kinetic energy of precipitation and runoff. For a flow rate of 12 L min<sup>-1</sup> and slope of 35%, the shear stress could reach up to 8 Pa. Furthermore, the equipment showed the effect of vegetation cover and slope on soil losses in different granulometric fractions (< 0.106 mm, 0.106 to 0.25 mm, 0.25 to 0.5 mm, 0.5 to 1.0 mm, 1.0 to 2.0 mm, and > 2.0 mm), revealing the potential of its use in several erosion studies on a laboratory scale.

**Keywords:** rainfall simulator; erosometer; Lithic Quartzipsamment; surface runoff.

### RESUMO

Diversos equipamentos foram desenvolvidos para a avaliação das perdas de solo por erosão hídrica. No entanto, raramente eles avaliam o efeito do impacto das gotas de chuva e do escoamento superficial em conjunto com a cobertura vegetal em diferentes declividades. Este estudo objetivou projetar e validar um equipamento, em escala de laboratório, para avaliar o efeito da erosão hídrica em amostras indeformadas de solo, bem como avaliar a velocidade de queda e tamanho das gotas de chuva simulada na superfície do solo e a intensidade do escoamento superficial em amostras com e sem cobertura vegetal. O equipamento é composto de um simulador de chuva, um suporte ajustável para diferentes declividades e alturas de queda e uma rampa de escoamento para testar amostras de solo indeformadas, com 15 x 20 x 40 cm (altura, largura e comprimento). Neste estudo, o equipamento simulou e avaliou o efeito da precipitação e do escoamento superficial nas perdas de solo, possibilitando a obtenção de diferentes valores de energia cinética de precipitação e escoamento. Para uma vazão de 12 L min<sup>-1</sup> e inclinação de 35%, a tensão de cisalhamento pode chegar a 8 Pa. Além disso, o equipamento evidenciou o efeito da cobertura vegetal e da declividade nas perdas de solo em diferentes frações granulométricas (< 0,106 mm, 0,106 a 0,25 mm, 0,25 a 0,5 mm, 0,5 a 1,0 mm, 1,0 a 2,0 mm, e > 2,0 mm), demonstrando o potencial do seu uso em diversos estudos de erosão em escala de laboratório.

**Keywords:** simulador de chuva; erosômetro; neossolo lítólico; escoamento superficial.

<sup>1</sup>Universidade Federal dos Vales de Jequitinhonha e Mucuri – Diamantina (MG), Brazil.

<sup>2</sup>Universidade Estadual Paulista “Júlio de Mesquita Filho” – Ilha Solteira (SP), Brazil.

Correspondence address: Bernat Vinolas Prat – Campus JK – Rodovia MGT 367 – Km 583, 5.000 – Alto da Jacuba – CEP 39100-000 – Diamantina (MG), Brazil. E-mail: bernat.vinolas@ict.ufvjm.edu.br

Conflicts of interest: the authors declare no conflicts of interest.

Funding: Coordination for the Improvement of Higher Education Personnel (CAPES), funding code 001; National Council for Scientific and Technological Development (CNPq); and Minas Gerais State Agency.

Received on: 02/14/2023. Accepted on: 06/16/2023

<https://doi.org/10.5327/Z2176-94781557>



This is an open access article distributed under the terms of the Creative Commons license.

## Introduction

Erosion is the leading global threat to soil degradation and food, water, and energy security. Projections indicate that water erosion could increase from 30 to 60% or more by 2070 (Borrelli *et al.*, 2020). Several factors affect soil losses through water erosion, such as rainfall erosivity and slope length, vegetation type and density, soil strength, and conservation practices (Bryan and Luk, 1981; Ran *et al.*, 2012; Aksoy *et al.*, 2013; Lassu *et al.*, 2015; Duarte *et al.*, 2021; Jin *et al.*, 2021).

Numerous studies aimed to quantify the influence of each of these parameters on soil losses by erosion (Seeger, 2007; Lassu *et al.*, 2015; Fernández-Raga *et al.*, 2019). Soil erosion research in the field has largely relied on standard plots that allow collecting water and sediments from surface runoff (Anache *et al.*, 2017; Bagarello *et al.*, 2018; Boardman and Evans, 2020). Standard plots are used to quantify the effects of plant cover and management practices on different soil, slope, and climate conditions (Chen *et al.*, 2018; Gao *et al.*, 2020; Klik and Rosner, 2020). However, the combined effects of these factors are difficult to test in the field, due to the costs and effort required in monitoring field experiments (Bryan and Luk, 1981). Additionally, these parameters vary in time and space, even within a single rainfall event (Zhao *et al.*, 2013; Lassu *et al.*, 2015).

Researches based on rainfall simulation can expand the knowledge about erosive process under different conditions (Cao *et al.*, 2014; Lassu *et al.*, 2015; Fernández-Raga *et al.*, 2019). Rainfall simulation is one of the most widely used methods in soil erosion studies (Seeger, 2007; Bertol *et al.*, 2012). The main objective is to produce simulated precipitations with intensity and duration control (Aksoy *et al.*, 2013; Iserloh *et al.*, 2013). Studies on rainfall simulation often require costly equipment and laborious installation and tests (Meyer, 2017; Dunkerley, 2021), which limit their application to numerous sites that would be required to grasp the effect of the different factors that cause soil erosion.

Laboratory studies, such as the Inderbitzen test, allow control over several variables that affect soil erosion, which would be almost impossible to achieve in field studies (Inderbitzen, 1961; Luk, 1977; Bryan and Luk, 1981; Fernández-Raga *et al.*, 2019). On the other hand, laboratory studies are a precursor and not a substitute for field experiments on a large scale. Still, they provide prior understanding, reduce complexity, time, and costs, and can increase field experiment efficiency (Lassu *et al.*, 2015).

The Inderbitzen test was introduced in Brazil in the 1970s to assess the stability of slopes based on soil erodibility (Inderbitzen, 1961; Silva and Melo, 2016). The equipment proposed by Inderbitzen in 1961 measured the erodibility of soils for geotechnical purposes and consisted basically of a flume that conducted runoff over the surface of a soil sample. Despite the possibility of evaluating different slope conditions and runoff intensities, the original equipment did not simulate the impact of raindrops on the soil surface, nor did it allow the evaluation

of factors effect that act on larger scales, such as vegetation cover and infiltration (Inderbitzen, 1961).

In order to simulate the effect of rainfall and expand the Inderbitzen test applications, the original procedure was improved throughout time by the development of modified equipment (Fácio, 1991; Silva and Melo, 2016). Despite the existence of numerous tests using modified Inderbitzen equipment, most of them are related to the simulation of soil erodibility for geotechnical purposes (Fácio, 1991; Bastos *et al.*, 1999; Soares *et al.*, 2018; Bandeira *et al.*, 2021; Stresser and Passini, 2023). As soil erosion is the object of study in several areas, including agronomy, geology, geography, and engineering, the development of a device that allows the direct evaluation of the various factors related to soil erosion and that provides reliable results is of the uttermost importance.

In this sense, the objective of the present study was to design and test a device to analyze factors related to water erosion in undisturbed soil samples, with or without surface vegetation at different slopes, evaluating both the impact of raindrops and water runoff.

## Material and Methods

### Modified Inderbitzen equipment

The proposed equipment consists of a support unit, a water storage tank, a runoff application unit, and the rainfall simulator unit (Figure 1).

Figure 2 details the measures of the support unit through its orthographic front and top views. This unit was made using square metallic tubes of the “Metalon” type with a section of 25 x 25 mm and a thickness of 2 mm. This component has elements for fixing the storage unit, the rainfall simulator, the undisturbed soil sample, and a plastic tray that collects runoff and sediments detached from the samples during the tests. The support unit allows the adjustment of two parameters that affect the kinetic energy of raindrops and runoff. The vertical distance of the sample surface to the rainfall simulator affects the fall height of the water drops and their velocity, allowing them to reach higher or lower kinetic energy depending on whether the sample is farther or closer to the rainfall simulator, respectively. The energy associated with surface runoff (shear stress), on the other hand, can be modified by the sample slope.

The water storage and application unit consist of a water reservoir (fed by a hose attached to the tap water source) and an opening with a small gutter that conducts the runoff evenly over the sample surface.

The rainfall simulation unit includes a water reservoir, hydraulic elements, and a motor used for uniform distribution of water drops over the sample. Rainfall is simulated using PVC pipes (nominal diameter 20 mm) perforated with 2 mm diameter holes. Figure 3 shows the bottom view of the arrangement of the holes in the pipes through which the water droplets exit, simulating a rainfall. The three rows of perforated pipes are 67 mm apart, with six holes in each row equally spaced by 67 mm.

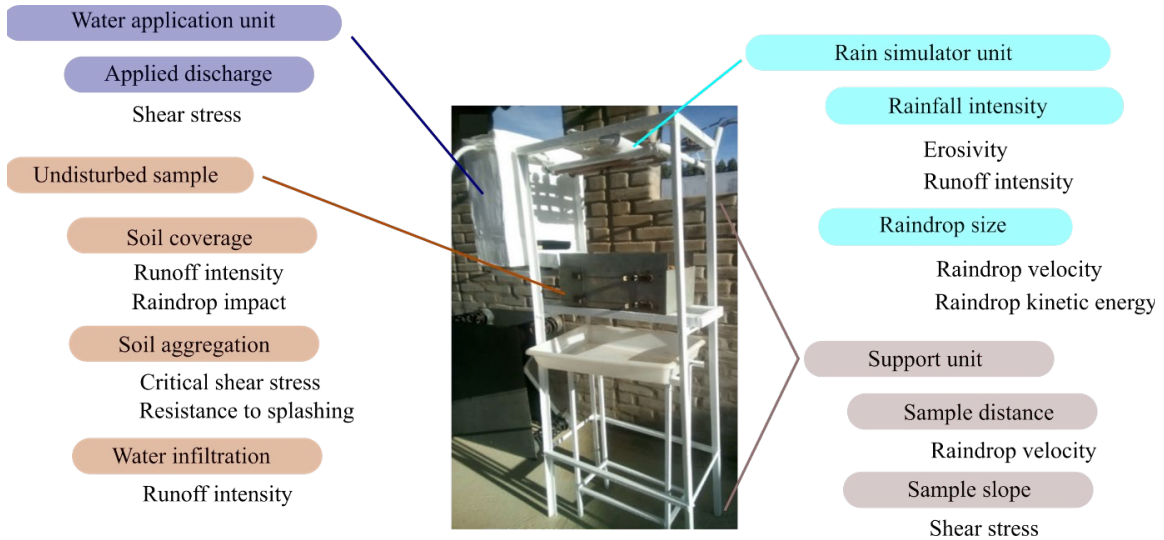


Figure 1 – Units and sample arrangements in the modified Inderbitzen equipment evaluated in this study.

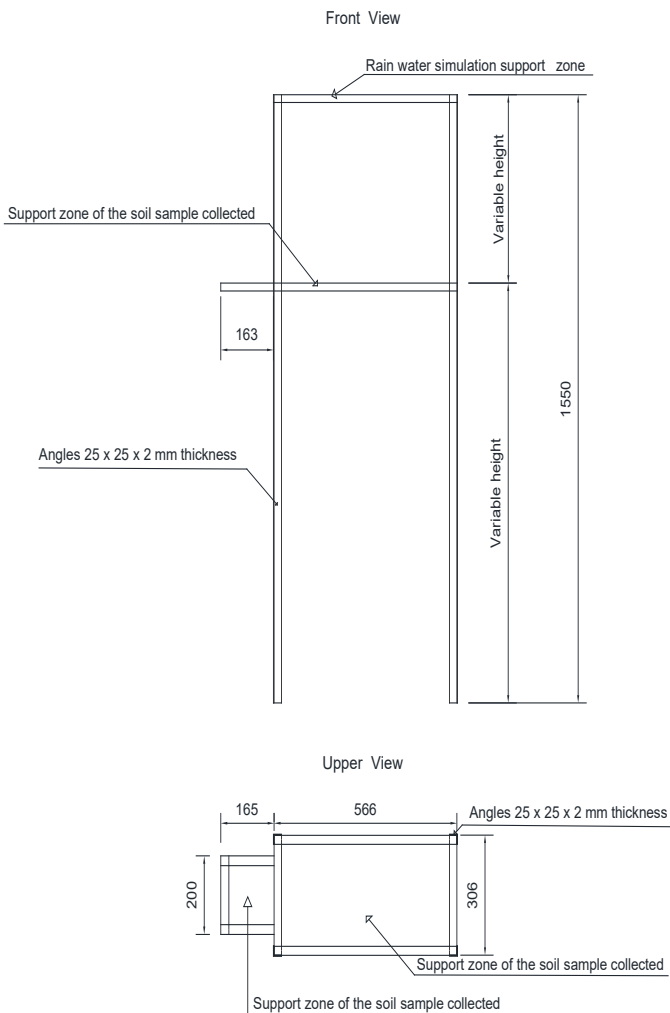


Figure 2 – Orthographic front and top view of the assembly structure (measurements in mm).

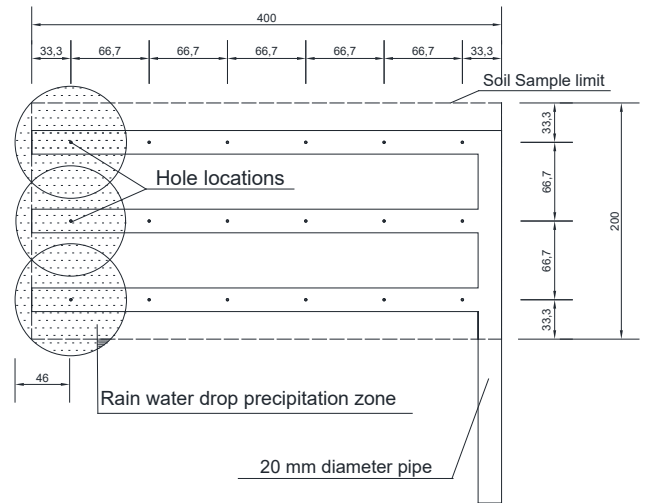


Figure 3 – Top view of the rainfall simulation unit component, showing the holes arranged along the pipe through which the simulated rainfall is applied (measurements in mm).

The set of perforated tubes is supported by an element that has a plane rotation with a turning radius of 46 mm. Thus, the water drops that exit through each hole reach the sample in a precipitation zone with an area equal to that of a circle with a radius of 46 mm ( $6,647.6 \text{ mm}^2$ ), as indicated by the shaded areas in Figure 3. This ensures that the drops can randomly fall at any point of the collected soil sample. The circular motion of the set of pipes is achieved with an electric motor attached to the top of the rainfall simulator, with a turning radius of 46 mm.

### Collection of undisturbed samples

The sampling system is composed of a U-shaped plate (Figures 4 and 5). After excavating the soil to the desired depth (0.15 m), this plate is inserted into one of the excavation walls using wooden blocks and a sledgehammer.



Figure 4 – (A) Soil sample collection with U-shaped plate and (B) soil sample prepared for evaluation.

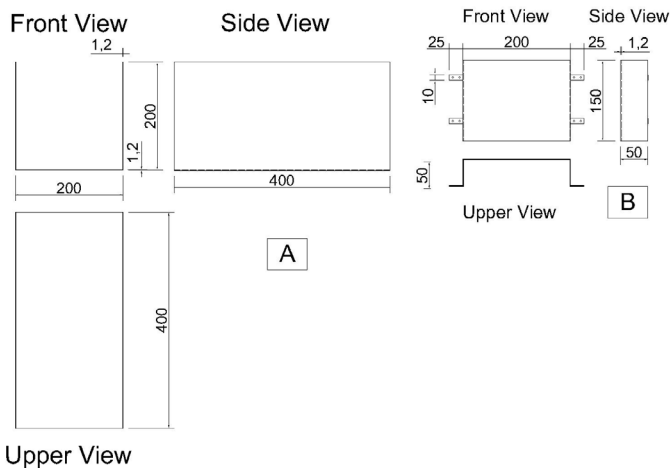


Figure 5 – Orthographic views of the (A) plate for soil sampling and (B) soil sample closure plate (all measurements in mm).

Once fully inserted, the plate accommodates the undisturbed soil sample inside. The smaller sides are then excavated, releasing the sample from the adjoining soil. Finally, the sample is lifted by hand and the open sides are closed with auxiliary plates (Figures 4 and 5).

The size of the samples and the collecting equipment were based on the following conditions:

- maximum sample weight of 40 kg, allowing sampling with fewer people and facilitating sample transportation;
- minimum sampling depth of 0.15 m, considered sufficient to adequately represent the phenomena that occur at the soil surface;
- specific mass of the wet soil of 2,500 kg m<sup>-3</sup>;
- rectangular shape with one side twice the size of the other.

Thus, measurements of 0.4 m and 0.2 m were adopted for the undisturbed sample, resulting in an area of 0.08 m<sup>2</sup>. The metal plate used to make the sample collection system was chosen according to Equation 1 (Arroyo et al., 2006) to determine the necessary thickness so that the maximum deformation arrow of the plate produced by the soil weight was 1 mm.

$$Arrow = \frac{5 p l_{sp}^4}{384 E I} \quad (1)$$

Where:

$p$ : the load applied to the plate per meter. The value of  $p$  is equal to 2,500 kg m<sup>-3</sup> x (0.15 m x 0.4 m) x 9.81 m s<sup>-2</sup> = 1471.5 N m<sup>-1</sup>;

$l_{sp}$ : the length of the smaller side of the plate (0.2 m);

$E$ : the modulus of deformation of the steel (210,000 N mm<sup>-2</sup> = 210 x 10<sup>9</sup> N m<sup>-2</sup>);

$I$ : the inertia of the sheet section used and is given by (Equation 2):

$$I = \frac{l_p^4 * thickness}{12} \quad (2)$$

Where:

$l_p$ : the length of the smaller side of the plate (0.4 m);

Thickness: the thickness of the metal plate (m).

For the designed conditions, the maximum arrow for a plate with thickness of 2 mm would be 0.74 mm, considered adequate according to the initial proposition of a maximum arrow of 1.0 mm.

### Characterization of simulated precipitation

The precipitation intensity ( $i$ ), is defined by the applied water discharge and the sample area (Equation 3).

$$i = \frac{60 * Q}{A} \quad (3)$$

Where:

$I$ : the precipitation intensity ( $\text{mm h}^{-1}$ );

$Q$ : the applied water discharge ( $\text{L min}^{-1}$ );

$A$ : the sample area ( $A = 0.2 \times 0.4 = 0.08 \text{ m}^2$ ).

For the samples employed in the present study, with a surface area of  $0.08 \text{ m}^2$ , a small water discharge of  $0.1 \text{ L min}^{-1}$  would already produce a precipitation intensity of  $75 \text{ mm h}^{-1}$ . Precipitation and runoff can be applied to different periods, with a collection of runoff and sediments at pre-established intervals. Inderbitzen tests are commonly performed every 30 minutes (Thoma et al., 2022). The kinetic energy of the precipitation depends on its intensity and duration (total precipitation). The raindrops produced by the simulator do not reach the sample surface at their terminal velocity due to the short distance traveled. Disregarding the interaction with the fluid environment during the fall, the terminal velocity of the falling particles could be calculated through Torricelli's equation (Equation 4).

$$v_f = \sqrt{v_0^2 + 2 a \Delta s} \quad (4)$$

Where:

$v_f$ : the final velocity of the particle in free fall ( $\text{m s}^{-1}$ );

$v_0$ : the initial velocity of the particle ( $\text{m s}^{-1}$ );

$a$ : the acceleration of gravity ( $9.81 \text{ m s}^{-2}$ );

$\Delta s$ : the distance traveled (m).

However, a particle in free fall in a fluid environment (such as the air) is subject not only to its weight but also to buoyancy and drag forces (Figure 6). So, the resultant force acting on the simulated raindrops is given by the difference between these acting forces (Equation 5).

$$F_R = F_p - F_E - F_A \quad (5)$$

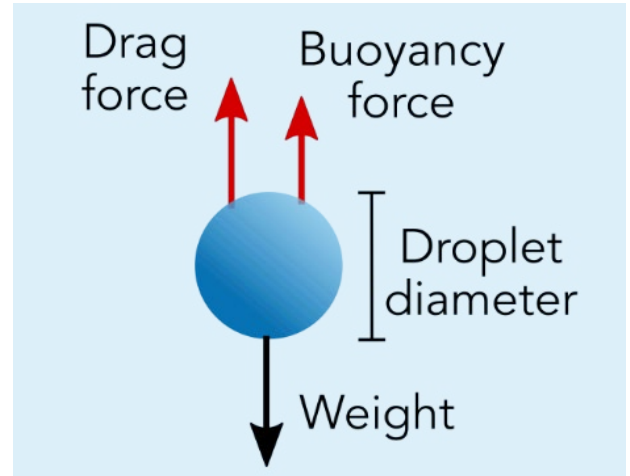


Figure 6 – Schematic representation of the forces acting on a spherical particle of diameter  $D$  in free fall in a fluid environment.

Where:

$F_R$ : the resultant force acting on the falling drop (N);

$F_p$ : the weight force (N);

$F_E$ : the buoyancy force (N);

$F_A$ : the drag force (N).

Once the resultant force is determined, the acceleration acting on the falling drops can be calculated by Equation 6. Hence, with the acceleration value, the velocity of the drops can be calculated for any falling distance by Equation 4.

$$F = m * a \quad (6)$$

Where:

$F$ : the force acting on a body (N);

$m$ : the mass of that body measured in kg;

$a$ : the acceleration measured in  $\text{m s}^{-2}$ .

The weight force is a consequence of gravity's action. If the resistive forces are not present, the acceleration of gravity increases the velocity along the entire path traveled according to Equation 4. The weight force acting on the falling particle can be calculated by Equation 7.

$$F_p = \rho_p V_p g \quad (7)$$

Where:

$F_p$ : the weight force (N);

$\rho_p$ : the specific mass of the particle ( $\rho_p = 1,000 \text{ kg m}^{-3}$  for water);

$V_p$ : the particle volume ( $V = \pi D^3/6$ , where  $D$  is the average droplet diameter);

$g$ : the acceleration of gravity ( $9.81 \text{ m s}^{-2}$ ).

Buoyancy is a resistive force with a value equal to the weight of the fluid volume displaced by the particle (Equation 8). In experimental conditions, its value is practically neglected since the fluid involved has a specific mass ( $\rho$ ) about 1,000 times smaller than the falling particle ( $\rho_{\text{air}} = 1.2 \text{ kg m}^{-3}$  and  $\rho_{\text{water}} = 1,000 \text{ kg m}^{-3}$  approximately).

$$F_E = \rho_f V_p g \quad (8)$$

Where:

$F_E$ : the buoyancy force (N);

$\rho_f$ : the specific mass of the fluid ( $\rho_{\text{air}} = 1.2 \text{ kg m}^{-3}$ );

$V_p$ : the particle volume ( $V_p = \pi D^3/6$ , where  $D$  is the average droplet diameter);

$g$ : the acceleration of gravity ( $9.81 \text{ m s}^{-2}$ ).

The drag force is more difficult to calculate since its value depends on the particle velocity, which in turn, depends on the value of the drag force to be measured. The drag force is calculated from the particle speed and its projection area (area of the circle in the case of droplets), as shown in Equation 9.

$$F_A = \frac{1}{2} \rho_f v^2 \frac{\pi D^2}{4} C_d \quad (9)$$

Where:

$F_A$ : the drag force (N);

$\rho_f$ : the specific mass of the fluid ( $\rho_f = 1.2 \text{ kg m}^{-3}$  for the air);

$v$ : the particle drop velocity ( $\text{m s}^{-1}$ );

$D$ : the average droplet diameter (m);

$C_d$ : the drag coefficient.

The drag coefficient is also a parameter that depends on the displacement velocity since it is calculated from the Reynolds number. The Reynolds number can be calculated by Equation 10, while the drag coefficient can be calculated according to the proposition of Cheng (2009), through Equation 11.

$$Re = \frac{v \rho_f D}{\mu} \quad (10)$$

Where:

$Re$ : the Reynolds number;

$v$ : the particle drop speed ( $\text{m s}^{-1}$ );

$\rho_f$ : the specific mass of the fluid ( $\rho_f = 1.2 \text{ kg m}^{-3}$  for the air);

$D$ : the average droplet diameter (m);

$\mu$ : the dynamic viscosity of the fluid ( $\mu = 1.75 \times 10^{-5} \text{ Pa.s}$  for the air).

$$C_d = \frac{24}{Re} (1 + 0.27Re)^{0.43} + 0.47 [1 - e^{(-0.04Re^{0.38})}] \quad (11)$$

Where:

$Re$ : the Reynolds number;

$C_d$ : the drag coefficient.

In order to determine the drag force, the drag coefficient, and the Reynolds number, the method of attempts was employed in the present study, using as initial estimates the velocities obtained through Equation 4, which disregards the interaction of the falling particle with the environment. From this baseline velocity estimate, the drag force (Equation 9) and the resultant force (Equation 5) were calculated. Therefore, the acceleration was calculated by Equation 6, and the droplet velocity by Equation 4. The velocities thus determined were used as initial estimates in a next attempt. The procedure was repeated five times, and the differences in the Reynolds number calculated between the initial estimated velocity and the final calculated velocity of the last attempt resulted in less than 1%, indicating that the velocity values achieved could be considered adequate.

The kinetic energy of each drop was calculated by Equation 12. The kinetic energy of the simulated precipitation was calculated from the product of the estimated number of drops (precipitation volume divided by the estimated volume of drops) by the kinetic energy of each drop, making it possible to obtain kinetic energy values in  $\text{MJ ha}^{-1} \text{ mm}^{-1}$ , which is the most commonly adopted unit in erosion studies (Morgan, 2005).

$$EC = \frac{1}{2} m v^2 \quad (12)$$

Where:

$EC$ : the kinetic energy of the droplet (J);

$m$ : the mass of the drop. Considering the density of water equal to 1.0,  $m$  is equal to the volume of the drop  $V_d$ . Considering perfectly spherical drops, the volume of the drops was calculated as  $V_d = \mu D^3/6$ , where  $D$  is the diameter of the drop.

$v$ : the velocity of the drop ( $\text{m s}^{-1}$ ).

The calculation routine employed assumed that the droplets were perfectly spherical and had a constant diameter. To evaluate the characteristics of the droplets produced, videos were taken through a camera with a resolution of 1,920 x 1,080 pixels and 30 frames per minute. The videos were processed with the Media Player application and images were captured every 1/30 of a second. These images were imported into the Autodesk AutoCAD 2020 application where the area of the droplets was measured. Finally, the equivalent droplet diameter was determined from the measured areas and assumed its perfectly spherical shape. The data thus obtained were fitted to frequency distributions employing the MASS package in R software (R Core Team, 2007). Subsequently, the fitted distributions and the observed data were subjected to the Kolmogorov-Smirnov test to verify that the fitted distributions were adequate.

### Characterization of simulated runoff

To characterize the surface runoff and determine the shear stress applied by the runoff, the methodology employed by several researchers for the evaluation of soil losses in canal waterways was applied (En-

riquez et al., 2015; Griebeler et al., 2005). The shear stress applied by the runoff in the bed of a canal can be determined by Equation 13.

$$\tau = \gamma R_h S \quad (13)$$

Where:

$\tau$ : the hydraulic shear stress (Pa);

$\gamma$ : the specific weight of water (9,810 N m<sup>-3</sup>);

$R_h$ : the hydraulic radius of the flow section. For large canal conditions, the hydraulic radius can be replaced by the flow depth itself, which would be more appropriate for surface flow conditions;

$S$ : the slope of the sample surface in the test (m/m).

The hydraulic radius depends on the flow section and the wetted perimeter. Both parameters are defined by the width of the flow bed sample and the depth of the flow. The depth of the flow can be estimated by Manning's equation for free surface flow (Equation 14, for rectangular canals). This equation can be solved numerically to determine the flow depth from the flow and canal characteristics (using the Microsoft Excel® Solver tool). The Reynolds number for the surface runoff was calculated by Equation 15.

$$\frac{n Q}{\sqrt{S}} = A R_h^{2/3} \rightarrow \frac{n Q}{S^{1/2}} = \frac{(p \cdot w)^{5/3}}{(2p + w)^{2/3}} \quad (14)$$

Where:

$Q$ : the flow rate of the runoff applied in the test (m<sup>3</sup> s<sup>-1</sup>);

$n$ : Manning's roughness coefficient (value for earthen canals in poor condition  $n = 0.025$  s m<sup>-1/3</sup>);

$S$ : the slope of the sample surface in the test;

$A$ : the area of the flow section, being equal to the product of the canal width and the flow depth;

$R_h$ : the hydraulic radius of the flow section, being given by the ratio between the area of the flow section and the area of the flow section and the wetted perimeter;

$p$ : the flow depth (m);

$w$  is the flow width, which was considered to be 0.2 m.

$$Re = \frac{v R_h}{\mu} \quad (15)$$

Where:

$Re$ : the Reynolds number;

$v$ : the flow velocity (m s<sup>-1</sup>);

**Table 1 - Physical characterization of the Lithic Quartzsammment used in the experiments.**

$\rho_r$	$\rho_g$	N	Granulometric distribution (mm)					
			> 2,0	2,0-1,0	1,0-0,5	0,5-0,25	0,2-0,106	< 0,106
--- kg m <sup>-3</sup> ---		m <sup>3</sup> m <sup>-3</sup>	----- g k <sup>-1</sup> -----					
2,450	1,460	0.40	14.2	48.1	222.1	656.8	48.7	10.1

$\rho_r$ : real specific mass or particle density;  $\rho_g$ : apparent specific mass or soil bulk density;  $n$ : void coefficient or total porosity.

$R_h$ : the hydraulic radius of the flow section being considered equal to flow depth for surface flow conditions;

$\mu$ : the kinematic viscosity of the fluid.

### Erodibility tests and equipment validation

For evaluation of soil loss and equipment validation, tests were performed on the modified Inderbitzen equipment. The tests were conducted at the Universidade Federal dos Vales do Jequitinhonha e Mucuri (UFVJM), in Diamantina/MG, with geographical coordinates of 18° 12' 13" S and 43° 34' 43" W and average altitude of 1,400 m.

Samples were collected from a Typic Quartzsammment (Table 1) according to the methodology presented in Soil Taxonomy (1999). They were collected with vegetation cover (spontaneous vegetation in the area) and without vegetation cover (removed before sampling). The vegetation cover is part of the Cerrado biome, with savanna and rupestrian field phytophysiognomies. The precipitation flow rate employed in the tests was 0.4 L min<sup>-1</sup>, resulting in an intensity of 300 mm h<sup>-1</sup>. In addition, the samples were subjected to surface runoff at a flow rate of 6 L min<sup>-1</sup>. Soil losses were expressed in g cm<sup>-2</sup> and soil loss rate in g cm<sup>-2</sup>min<sup>-1</sup>; these units are the most commonly employed in studies with Inderbitzen equipment. The trials were conducted at three different slopes, 5%, 17.5%, and 35%. The runoff from the tests and the eroded material were collected 1, 5, 10, 15, 20, and 30 minutes after the test started. The eroded material was sedimented, collected, oven dried, and sieved. The following particle size fractions were quantified: < 0.106 mm, 0.106 to 0.25 mm, 0.25 to 0.5 mm, 0.5 to 1.0 mm, 1.0 to 2.0 mm, and > 2.0 mm. After drying, the material from each fraction was weighed.

The tests were performed in triplicate, totaling 18 samples (2 surface conditions x 3 slopes x 3 repetitions). The data were submitted to variance analysis and comparison of means tests (Tukey test at 5% significance level) when significant effects of any source of variation were observed. The statistical analyses were performed in R software (R Core Team, 2007).

## Results and Discussion

### Rainfall characterization

Varying the distance from the sample to the rainfall simulator allowed a wide range of droplet velocities (Figure 7). The terminal velocity of the drops is reached when the resultant of the forces acting on the falling particle (Figure 8) is null. For the conditions evaluated in this study, we found terminal velocity values of 6.11; 7.71; 8.45; and 8.91 m s<sup>-1</sup> for drops with diameters 2; 3; 4, and 5 mm, respectively.

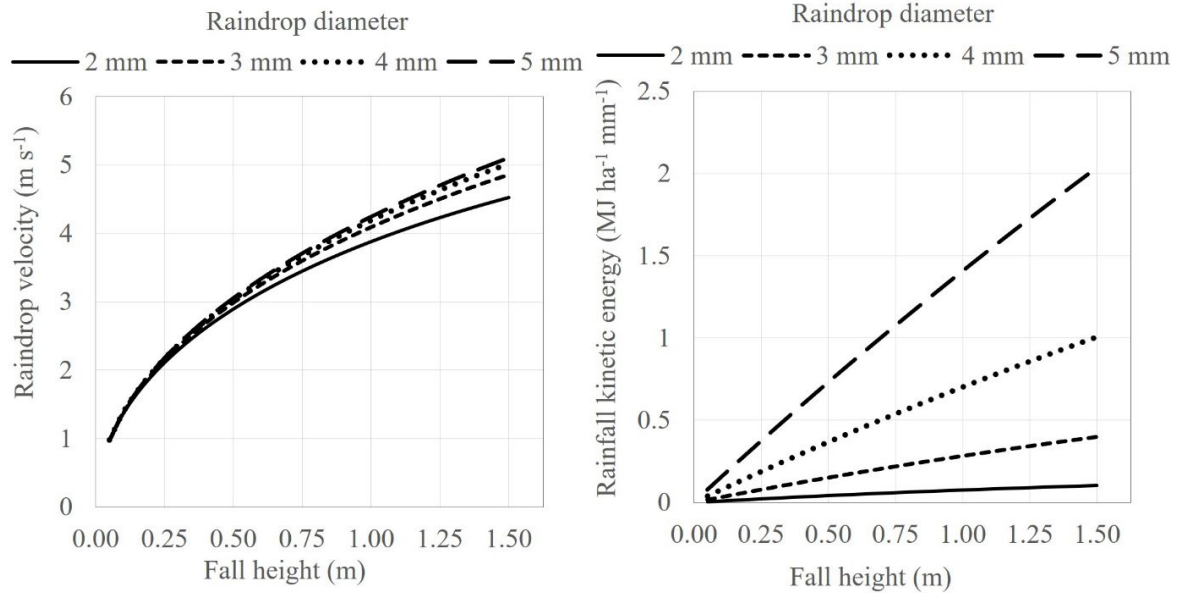


Figure 7 – Relationship between droplet velocity, precipitation kinetic energy, and drop height.

These velocities are higher than those obtained for the rainfall simulator considering the range of distances from 0.5 to 1.50 m (Figure 7), which indicates that the simulated erosivity would be lower than that of natural rainfall at the same intensity.

At heights of 0.5 m, the drops reach the soil surface at velocities of about 3.0 m s<sup>-1</sup>. By increasing the vertical distance of the sample to 1.0 m, the drops reach the surface at velocities of 3.9 to 4.2 m s<sup>-1</sup> depending on the drop diameter. Velocities above 5 m s<sup>-1</sup> are reached only by larger drops (4 and 5 mm diameter) and with a drop height of 1.5 m. At these drop heights (0.5 to 1.5 m), the differences in velocity due to different droplet diameters are small, while the kinetic energy of precipitation is markedly different (Figure 7). For the 0.5 m drop height, for example, the kinetic energy of precipitation varied from 0.04 to 0.73 MJ ha<sup>-1</sup> mm<sup>-1</sup> as the droplet diameter increased from 1 to 5 mm – a difference of 1,700%. The range of variation in kinetic energy is wider because it depends on the mass of the falling drops and increases with the square of the velocity (Equation 12), which amplifies its effect.

The precipitation generated during the equipment validation tests presented a mean droplet diameter of 2.72 mm, with a range of variation from 1.36 to 6.04 mm. As shown in Figure 8, the distribution was slightly asymmetric to the right, with the median (2.46 mm) lower than the mean. The drop size distribution fitted a gamma-type distribution, with a shape parameter equal to 10.6 and a rate of 3.9 (Figure 8).

**Runoff characterization**

Variations in runoff flow rate and sample slope allowed different shear stress values (Figure 9). For flow rates from 1 to 12 L min<sup>-1</sup>, the Reynolds number ranged from 93 to 1,120. This indicates a transition to turbulent flow regime, with progressive increase of inertial forces over resistive forces (viscosity) as the applied flow rate increases (Equation 14).

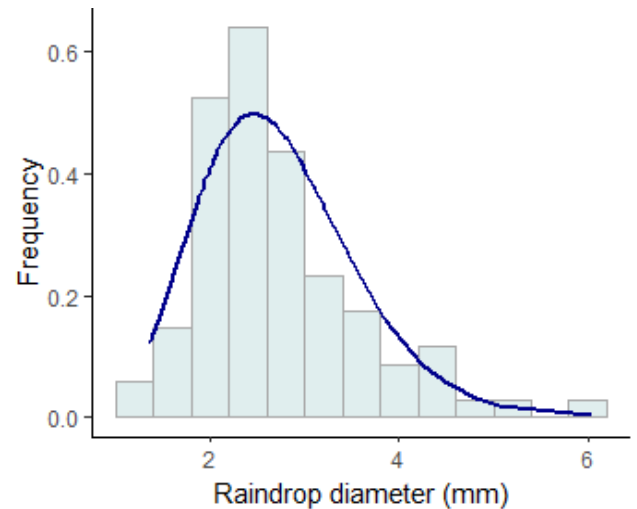


Figure 8 – Observed distribution of the droplet diameter generated by the rainfall simulator (vertical bars) and fitted distribution (gamma distribution with shape equal to 10.6 and rate of 3.9).

According to Silva and Melo (2016), in a synthesis of several papers related to the evaluation of erodibility with the Inderbitzen test, the flow rates used were between 3 and 18.8 L min<sup>-1</sup>, with average value of 6 L min<sup>-1</sup>. The hydraulic shear stress applied by the surface runoff over the sample surface was markedly affected by the slope (Figure 9). For the 5% slope, the flow rate had little effect on the shear stress exerted by the runoff, ranging from 0.5 to 2.1 Pa for flow rates of 1 to 12 L min<sup>-1</sup>. On the other hand, for the 35% slope, the shear stress amplitude as a function of the flow rate was much larger, varying from 1.8 to 8.2 Pa for flow rates from 1 to 12 L min<sup>-1</sup>.

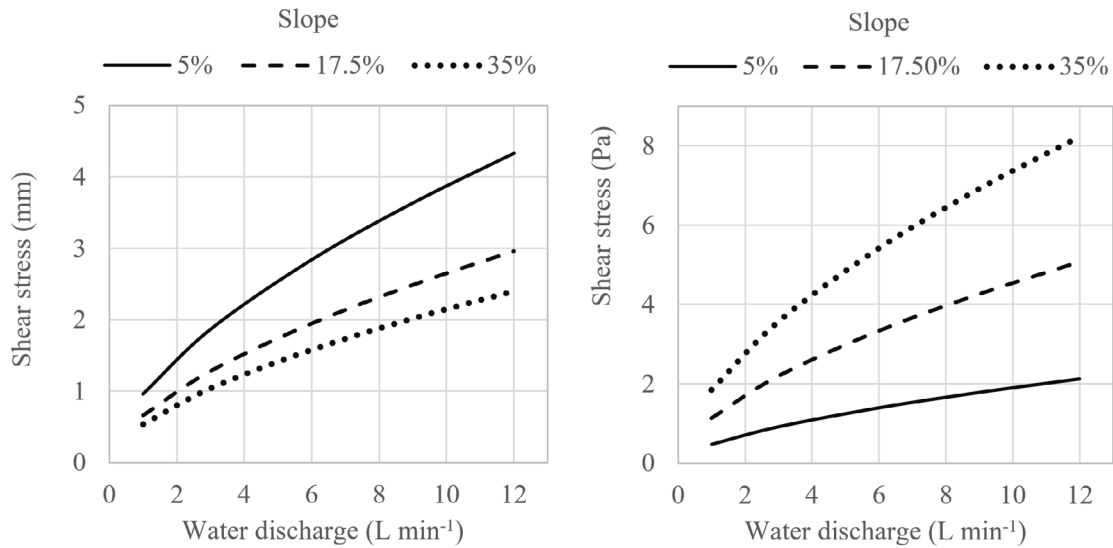


Figure 9 – Depth of surface runoff and hydraulic shear stress applied on the samples surface by the runoff.

### Soil losses during the tests

The sediment eroded during the tests in the modified Inderbitzen test presented a particle size distribution significantly different from the original soil (Figure 10). While the original soil showed a wide predominance of coarser fractions (about 94% of the particles were larger than 0.25 mm), the eroded sediment consisted mainly of thinner fractions, with about 60% of the material having a diameter smaller than 0.25 mm. The finest fraction (< 0.106 mm) presented 8–15 times higher contents in the collected sediments than in the original soil, while the 0.106–0.25 mm fraction showed 10–12 times higher contents in the sediments. This process of fine material loss causes some implications, such as a marked reduction in soil fertility since the colloidal material retains nutrients and the aggravation of water erosion off-site effects since these smaller particles have less resistance to transport, being more easily carried over longer distances.

The evolution of losses throughout the test was also markedly different depending on the particle size fraction considered (Figure 11). The largest losses were continuously observed in the fractions from 0.25 to 0.5 mm and 0.106 to 0.25 mm. The loss of the other fractions was generally below 0.05 g cm<sup>-2</sup> after 30 minutes of testing for all surface cover and slope conditions. The fraction with diameter smaller than 0.106 mm, despite being thinner and therefore more easily transported, showed very low loss values due to the originally very low soil contents of only 1% (Table 1).

In the condition without vegetation cover, besides the differences in the amount of soil loss at each slope (Table 2), the granulometric fractions also exhibited distinct behavior (Figure 11). On the slopes of 5% and 17.5%, the losses for the fraction from 0.106 to 0.25 mm remained far from the others, while on the 35% slope, this fraction and the 0.25 to 0.5 mm showed similar behavior to each other and markedly different in relation to the other fractions.

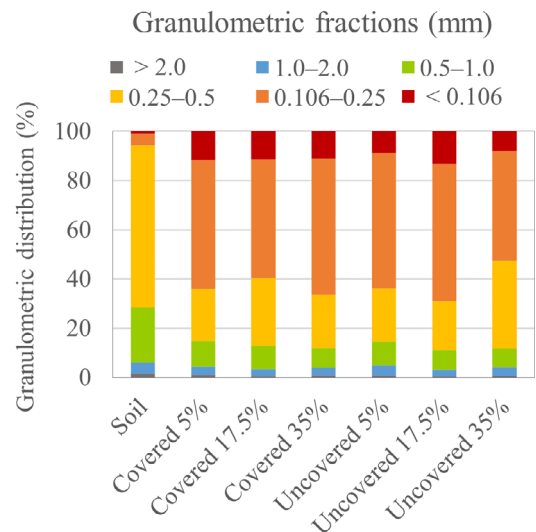


Figure 10 – Particle size composition of the Lithic Quartzipsamment and sediment eroded during the modified Inderbitzen equipment tests for different soil cover conditions and slope.

In the condition with vegetation cover, losses were always below 0.1 g cm<sup>-2</sup> on the 5% and 17.5% slopes. On the 35% slope, the losses increased sharply throughout the test, especially in the fraction from 0.106 to 0.25 mm.

Significant effects of ground cover on the soil surface and slope on the identified soil losses in the different fractions were observed (Table 2). However, the interaction between these two factors was not significant for any particle size fraction. The general trend observed for total losses (sum of all fractions) was maintained for most fractions. As for total losses, the fractions 0.25 to 0.106 mm, 0.25 to 0.5 mm, 0.5 to 1.0 mm, and 1.0 to 2.0 mm showed significantly higher losses in the condition without vegetation cover and at a slope of 35%, while losses at 5% and 17.5% did not differ.

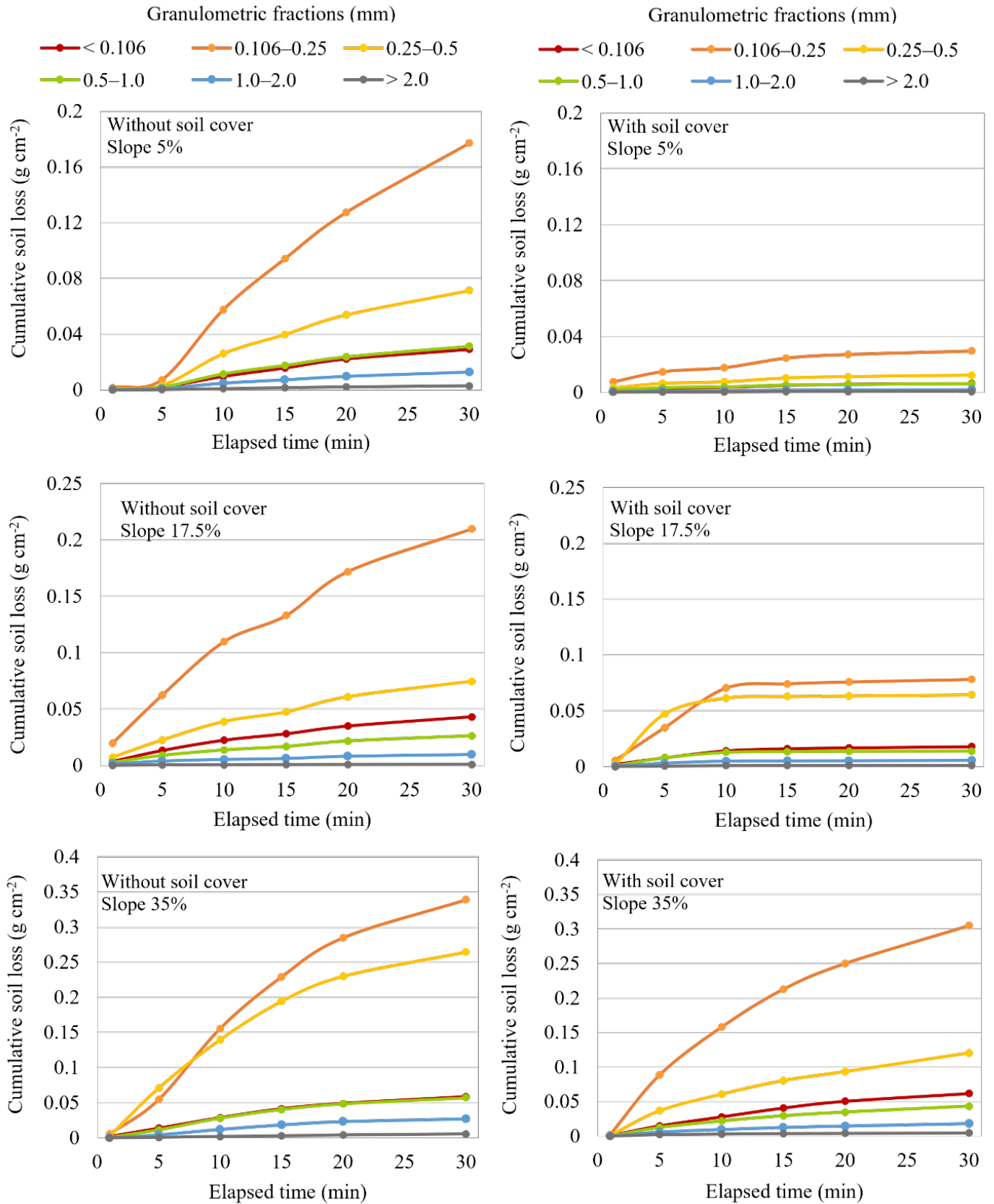


Figure 11 – Cumulative soil losses throughout the modified Inderbitzen trials.

**Table 2 – Average soil losses (g cm<sup>-2</sup>) for typical lithologic lithosols in the simulated erosion tests using the modified Inderbitzen equipment.**

Slope (%)	> 2.0	2.0–1.0	1.0–0.5	0.5–0.25	0.25–0.106	< 0.106	Total
	Without vegetation cover						
5	0.003 Ab	0.013 Ab	0.031 Ab	0.071 Ab	0.177 Ab	0.029 Ab	0.325 Ab
17.5	0.001 Ab	0.010 Ab	0.026 Ab	0.075 Ab	0.210 Ab	0.043 Aab	0.365 Ab
35	0.006 Aa	0.027 Aa	0.057 Aa	0.265 Aa	0.339 Aa	0.059 Aa	0.752 Aa
	With vegetation cover						
5	0.001 Ab	0.002 Bb	0.006 Bb	0.013 Bb	0.030 Ab	0.006 Ab	0.058 Bb
17.5	0.001 Ab	0.005 Bb	0.014 Bb	0.064 Bb	0.078 Ab	0.018 Aab	0.180 Bb
35	0.005 Aa	0.018 Ba	0.043 Ba	0.121 Ba	0.305 Aa	0.062 Aa	0.554 Ba

For the coarser fraction (> 2.0 mm), the effect of vegetation cover was not significant, only the slope, with higher losses also on the 35% slope. The losses of the finest fraction (< 0.106 mm) also did not show a significant effect of vegetation cover, but the slopes differed from each other more markedly, with a gradation of losses in 5% < 17.5% < 35%.

Averages followed by the same letter do not differ using Tukey's test at a 5% significance level. Capital letters compare vegetation cover and lowercase letters compare slopes.

## Conclusions

The proposed equipment allowed obtaining different values of the kinetic energy of precipitation and erosivity from changes in the distance of the samples in the simulator and in the precipitation intensity.

Different shear stresses could be applied by surface runoff from variations in runoff flow and sample slope. For a flow rate of 12 L min<sup>-1</sup>

and slope of 35%, the shear stress could reach up to 8 Pa. The proposed methodology allowed the collection of undeformed soil samples with dimensions of 0.40 m length, 0.20 m width, and 0.15 m depth, enabling the maintenance of vegetation cover over the collected soil surface. In the simulated erosion tests, the equipment allowed the effect of vegetation cover and slope on soil losses in different granulometric fractions to be highlighted, indicating the possibility of its use in laboratory erosion studies.

This study allowed for the design and testing of the equipment to analyze factors related to water erosion in undisturbed soil samples. It evaluated the impact of raindrops and runoff on samples with and without surface vegetation, as well as on different slopes. Finally, this new equipment can assist researchers in the laboratory conducting analyses of soil erosion by reducing the need for laborious analysis in the field. Consequently, it would lead to cost reduction and shorter research periods concerning soil erosion issues.

## Contribution of authors:

THOMA, A. C.: Data curation; Formal Analysis; Investigation; Validation; Methodology; Resources; Validation; Writing – original draft. TASSINARI, D.: Data curation; Formal Analysis; Investigation; Methodology; Supervision; Validation; Visualization; Writing – original draft; Writing – review & editing. PRAT, B. V.: Conceptualization; Data curation; Formal Analysis; Investigation; Methodology; Project administration; Resources; Supervision; Validation; Visualization; Writing – original draft; Writing – review & editing. SANTOS, L. L.: Data curation; Formal Analysis; Investigation; Supervision; Validation; Visualization; Writing – original draft. SILVA, B. P. C.: Data curation; Formal Analysis; Investigation; Supervision; Validation; Visualization; Writing – review & editing. SILVA, A. C.: Data curation; Formal Analysis; Funding; Acquisition; Investigation; Methodology; Project administration; Resources; Supervision; Validation; Visualization; Writing – review & editing.

## References

- Aksoy, H.; Erdem Unal, N.; Cokgor, S.; Gedikli, A.; Yoon, J.; Koca, K.; Inci, S. B.; Eris, E.; Pak, G., 2013. Laboratory experiments of sediment transport from bare soil with a rill. *Hydrological Sciences Journal*, v. 58, (7), 1505-1518. <https://doi.org/10.1080/02626667.2013.824085>.
- Anache, J.A.; Wendland, E.C.; Oliveira, P.T.; Flanagan, D.C.; Nearing, M.A., 2017. Runoff and soil erosion plot-scale studies under natural rainfall: A meta-analysis of the Brazilian experience. *Catena*, v. 152, 29-39. <https://doi.org/10.1016/j.catena.2017.01.003>.
- Arroyo, J.C.; Corres, G.; García-Rosales, G.; Romana, M.G.; Romero, A.; Sánchez, R.; Teja, Ó. (2006). *Números gordos en el proyecto de estructuras*. Madrid.
- Bagarello, V.; Ferro, V.; Keesstra, S.; Comino, J.R.; Pulido, M.; Cerdà, A., 2018. Testing simple scaling in soil erosion processes at plot scale. *Catena*, v. 167, 171-180. <https://doi.org/10.1016/j.catena.2018.04.035>.
- Bandeira, A.P.N.; Macedo, C.C.A.; Clarindo, G.S.; Lima, M.G.S.; Souza Neto, J.B., 2021. Assessment of potential surface degradation resulting from erosion processes in environmentally protected area. *Soils and Rocks*, v. 44, (1), e2021052420. <https://doi.org/10.28927/SR.2021.052420>.
- Bastos, C.A.B., 1999. *Estudo geotécnico sobre a erodibilidade de solos residuais não saturados*. Tese de Doutorado, Universidade Federal do Rio Grande do Sul, Porto Alegre.

- Bertol, I.; Bertol, C.; Barbosa, F.T., 2012. Simulador de chuva tipo empuxo com braços movidos hidráulicamente: fabricação e calibração. *Revista Brasileira de Ciência do Solo*, v. 36, (6), 1905-1910. <https://doi.org/10.1590/s0100-06832012000600024>.
- Boardman, J.; Evans, R., 2020. The measurement, estimation and monitoring of soil erosion by runoff at the field scale: Challenges and possibilities with particular reference to Britain. *Progress in Physical Geography: Earth and Environment*, v. 44, (1), 31-49. <https://doi.org/10.1177/0309133319861833>.
- Borrelli, P.; Robinson, D.A.; Panagos, P.; Lugato, E.; Yang, J.E.; Alewell, C.; Wuepper, D.; Montanarella, L.; Ballabio, C., 2020. Land use and climate change impacts on global soil erosion by water (2015-2070). *Proceedings of the National Academy of Sciences*, v. 117, (36), 21994-22001. <https://doi.org/10.1073/pnas.2001403117>
- Bryan, R.B.; Luk, S.H., 1981. Laboratory experiments on the variation of soil erosion under simulated rainfall. *Geoderma*, v. 26, (4), 245-265. [https://doi.org/10.1016/0016-7061\(81\)90023-9](https://doi.org/10.1016/0016-7061(81)90023-9).
- Cao, L.X.; Zhang, K.L.; Liang, Y., 2014. Factors affecting rill erosion of unpaved loess roads in China. *Earth Surface Processes and Landforms*, v. 39, (13), 1812-1821. <https://doi.org/10.1002/esp.3569>.
- Chen, H.; Zhang, X.; Abla, M.; Lü, D.; Yan, R.; Ren, Q.; Yang, Y.; Zhao, W.; Lin, P.; Liu, B.; Yang, X., 2018. Effects of vegetation and rainfall types on surface runoff and soil erosion on steep slopes on the Loess Plateau, China. *Catena*, v. 170, 141-149. <https://doi.org/10.1016/j.catena.2018.06.006>.
- Cheng, N.S., 2009. Comparison of formulas for drag coefficient and settling velocity of spherical particles. *Powder Technology*, v. 189, (3), 395-398. <https://doi.org/10.1016/j.powtec.2008.07.006>.
- Duarte, M.L.; Sousa, J.A.P.; Castro, A.L.; Lourenço, R.W., 2021. Dynamics of land use in a rural settlement in the Brazilian Legal Amazon. *Brazilian Journal of Environmental Sciences*, v. 56, (3), 375-384. <https://doi.org/10.5327/z217694781005>.
- Dunkerley, D., 2021. The case for increased validation of rainfall simulation as a tool for researching runoff, soil erosion, and related processes. *Catena*, v. 202, 105283. <https://doi.org/10.1016/j.catena.2021.105283>.
- Enriquez, A.G.; Silva, D.P.D.; Pruski, F.F.; Griebeler, N.P.; Cecon, P.R., 2015. Erodibilidade e tensão crítica de cisalhamento no canal de drenagem de estrada rural não pavimentada. *Revista Brasileira de Engenharia Agrícola e Ambiental*, v. 19, 160-165. <https://doi.org/10.1590/1807-1929/agriambi.v19n2p160-165>.
- Fácio, J.A., 1991. Proposição de uma metodologia de estudo da erodibilidade dos solos do Distrito Federal. *Dissertação (Mestrado em Geotecnia)*, Universidade de Brasília, Brasília.
- Fernández-Raga, M.; Campo, J.; Rodrigo-Comino, J.; Keesstra, S.D., 2019. Comparative analysis of splash erosion devices for rainfall simulation experiments: a laboratory study. *Water*, v. 11, (6), 1228. <https://doi.org/10.3390/w11061228>.
- Gao, J.; Bai, Y.; Cui, H.; Zhang, Y., 2020. The effect of different crops and slopes on runoff and soil erosion. *Water Practice and Technology*, v. 15, (3), 773-780. <https://doi.org/10.2166/wpt.2020.061>.
- Griebeler, N.P.; Pruski, F.F.; Mehl, H.U.; Silva, D.D.D.; Oliveira, L.F., 2005. Equipamento para determinação da erodibilidade e tensão crítica de cisalhamento do solo em canais de estradas. *Revista Brasileira de Engenharia Agrícola e Ambiental*, v. 9, (2), 166-170. <https://doi.org/10.1590/s1415-43662005000200003>.
- Inderbitzen, A.L., 1961. An erosion test for soils. *Materials Research & Standards*, v. 1, 553-554.
- Iserloh, T.; Ries, J.B.; Arnáez, J.; Boix-Fayos, C.; Butzen, V.; Cerdà, A.; Echeverría, M.T.; Fernández-Gálvez, J.; Fister, W.; Geißler, C.; Gómez, J.A.; Gómez-Macpherson, H.; Kuhn, N.J.; Lázaro, R.; León, F.J.; Martínez-Mena, M.; Martínez-Murillo, J.F.; Marzen, M.; Mingorance, M.D.; Ortigosa, L.; Peters, P.; Regüés, D.; Ruiz-Sinoga, J.D.; Scholten, T.; Seeger, M.; Solé-Benet, A.; Wengel, R.; Wirtz, S., 2013. European small portable rainfall simulators: A comparison of rainfall characteristics. *Catena*, v. 110, 100-112. <https://doi.org/10.1016/j.catena.2013.05.013>.
- Jin, F.; Yang, W.; Fu, J.; Li, Z., 2021. Effects of vegetation and climate on the changes of soil erosion in the Loess Plateau of China. *Science of The Total Environment*, v. 773, 145514. <https://doi.org/10.1016/j.scitotenv.2021.145514>.
- Klik, A.; Rosner, J., 2020. Long-term experience with conservation tillage practices in Austria: Impacts on soil erosion processes. *Soil and Tillage Research*, v. 203, 104669. <https://doi.org/10.1016/j.still.2020.104669>.
- Lassu, T.; Seeger, M.; Peters, P.; Keesstra, S. D., 2015. The Wageningen rainfall simulator: Set-up and calibration of an indoor nozzle-type rainfall simulator for soil erosion studies. *Land Degradation & Development*, v. 26, (6), 604-612. <https://doi.org/10.1002/ldr.2360>.
- Luk, S.H., 1977. Rainfall erosion of some Alberta soils: A laboratory simulation study. *Catena*, v. 3, (3-4), 295-309. [https://doi.org/10.1016/0341-8162\(77\)90035-2](https://doi.org/10.1016/0341-8162(77)90035-2).
- Meyer, L.D., 2017. Rainfall Simulators for Soil Erosion Research. In: Lal, R. (Ed.). *Soil Erosion Research Methods*. Routledge, Abingdon-on-Thames, 83-104. <https://doi.org/10.1201/9780203739358-4>.
- Morgan, R.P.C., 2005. *Soil Erosion and Conservation*. Oxford: Blackwell Science.
- Ran, Q.; Su, D.; Li, P.; He, Z., 2012. Experimental study of the impact of rainfall characteristics on runoff generation and soil erosion. *Journal of Hydrology*, v. 424-425, 99-111. <https://doi.org/10.1016/j.jhydrol.2011.12.035>.
- Seeger, M., 2007. Uncertainty of factors determining runoff and erosion processes as quantified by rainfall simulations. *Catena*, v. 71, (1), 56-67. <https://doi.org/10.1016/j.catena.2006.10.005>.
- Silva, A.P.N.; Melo, M.T.S., 2016. Análise do Histórico de Desenvolvimento de Modelos de Aparelho de Inderbitzen para a Confecção de Tabelas Comparativas. In: Neves, A.F.; Paula, M.H.; Anjos, P.H.R.; Silva, A.G. (Eds.). *Estudos Interdisciplinares em Ciências Biológicas, Saúde, Engenharias e Gestão*. São Paulo, Blucher, pp. 51-64.
- Soares, D.L.; Polivanov, H.; Barroso, E.V.; Motta, L.M.G.; Souza, C.C., 2018. Erodibilidade de Solos em Taludes de Corte de Estrada Não Pavimentada. *Anuário do Instituto de Geociências*, v. 41, (1), 179-193. [https://doi.org/10.11137/2018\\_1\\_179\\_193](https://doi.org/10.11137/2018_1_179_193).
- Soil Taxonomy (1999). A basic system of soil classification for making and interpreting soil surveys. *Agriculture Handbook 436 (rev.)*.
- Stresser, C.; Passini, L.B., 2023. Soil Erodibility Rates through a Hydraulic Flume Erosometer: Test Assembly and Results in Sandy and Clayey Soils. *Open Journal of Civil Engineering*, v. 13, (1), 155-170. <https://doi.org/10.4236/ojce.2023.131011>.
- Team, R.D.C., 2007. R: A language and environment for statistical computing. Vienna, R Foundation for Statistical Computing (Accessed July 31, 2023). Available at <https://www.R-project.org/>.
- Thoma, A.C.; Tassinari, D.; Prat, B.V.; Fernandes, J.S.C.; Silva, A.C., 2022. Erodibilidade de Neossolo Litólico pelo ensaio de Inderbitzen modificado e eficiência de blocos de solo-cimento para controle da erosão hídrica. *Engenharia Sanitária e Ambiental*, v. 27, 511-522. <https://doi.org/10.1590/S1413-415220210099>.
- Zhao, G.; Mu, X.; Wen, Z.; Wang, F.; Gao, P., 2013. Soil erosion, conservation, and eco-environment changes in the Loess Plateau of China. *Land Degradation & Development*, v. 24, (5), 499-510. <https://doi.org/10.1002/ldr.2246>.